Ultraluminous X-ray sources - new distance indicators?

Agata Różańska, CAMK PAN
Karol Bresler, Bartosz Bełdycki, Jerzy Madej, Tek P. Adhikari

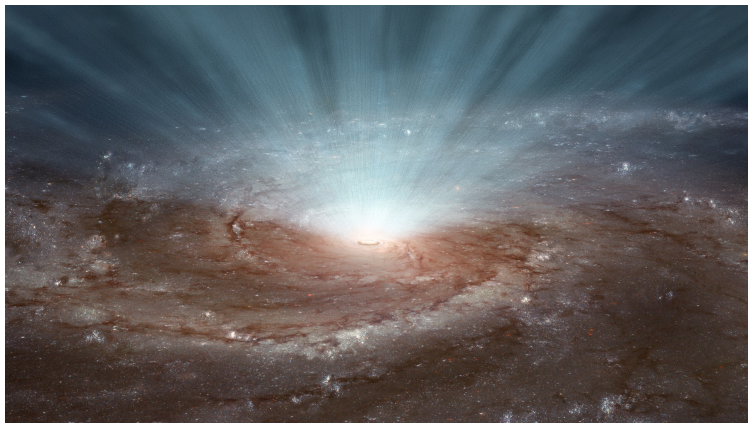

26.09.2018, Palermo, Italy

Observations of accreting sources

X-ray binaries: Zhang +00, GRS 19151+105

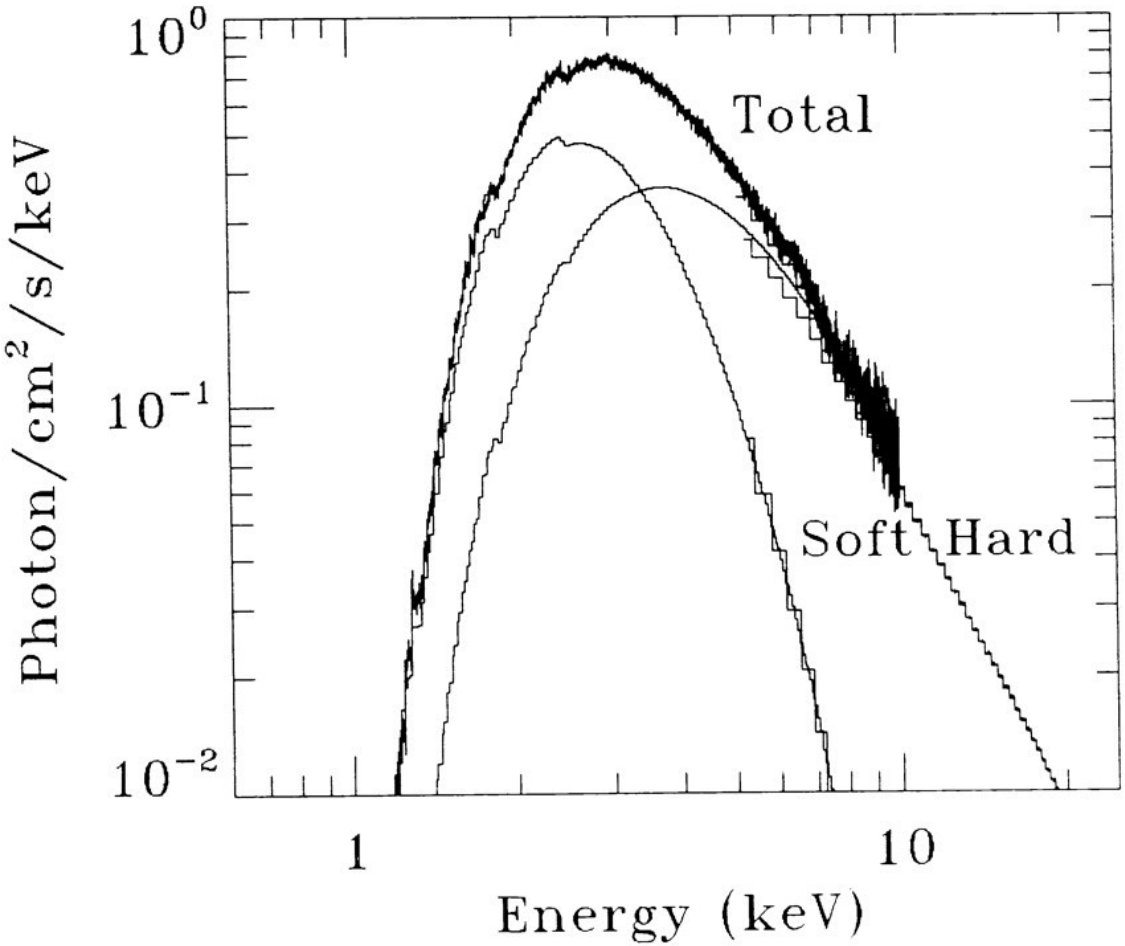

Observations of accreting sources

X-ray binaries: Kolehmainer +11, GX 339-4

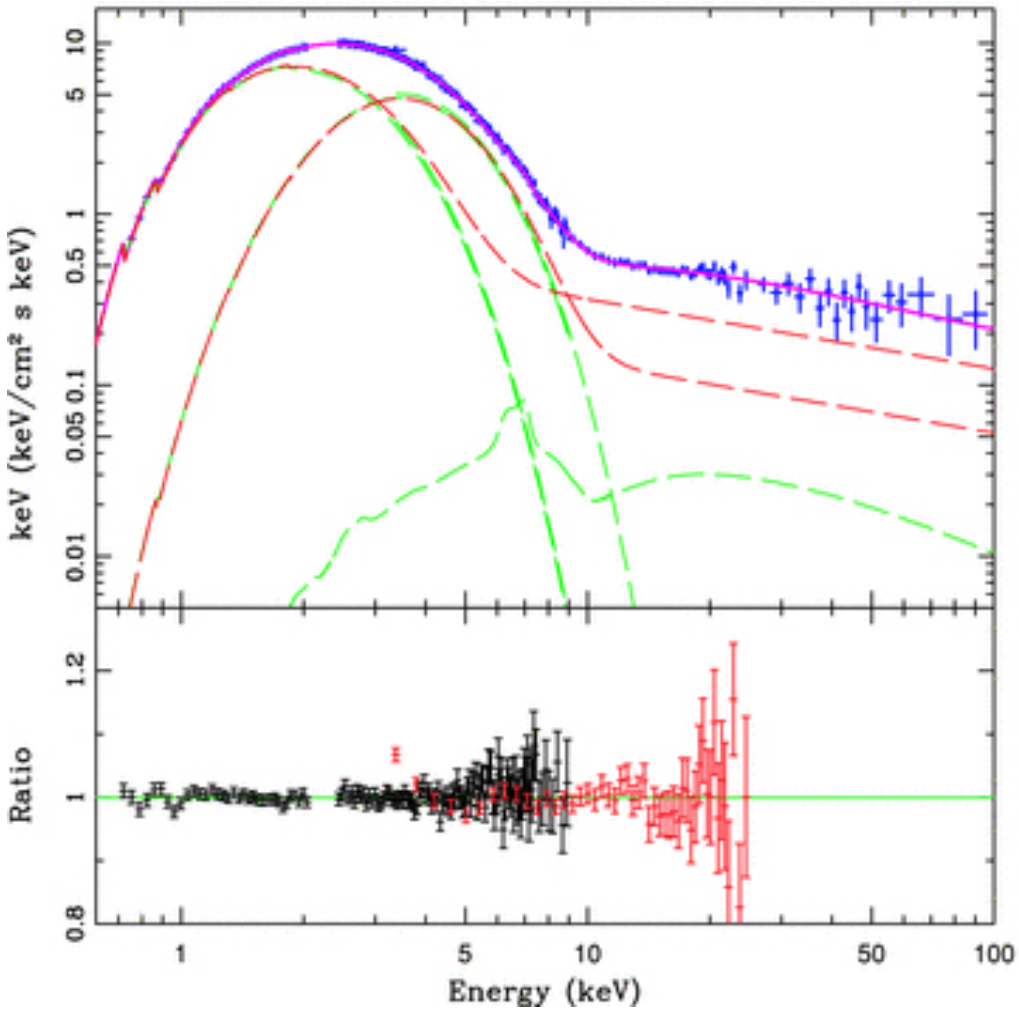

Observations of accreting sources

Seyfert galaxies: Jin +12, J112328+052823, PG 1415+451

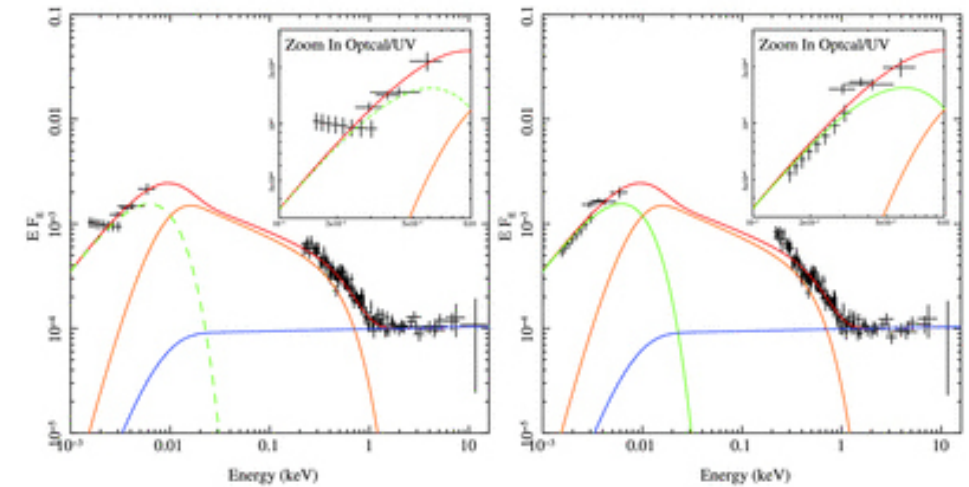

(d)

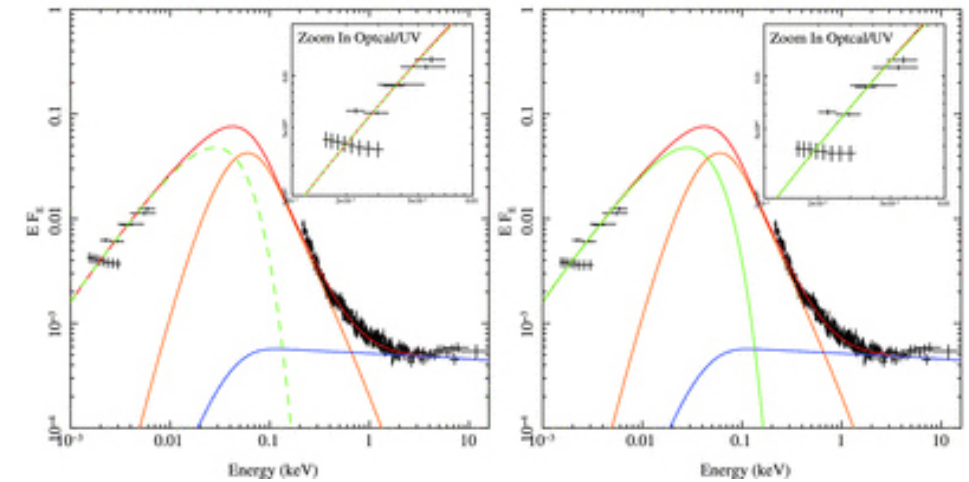

Observations of accreting sources

ULX sources: Walton +15, Holmberg II X-1

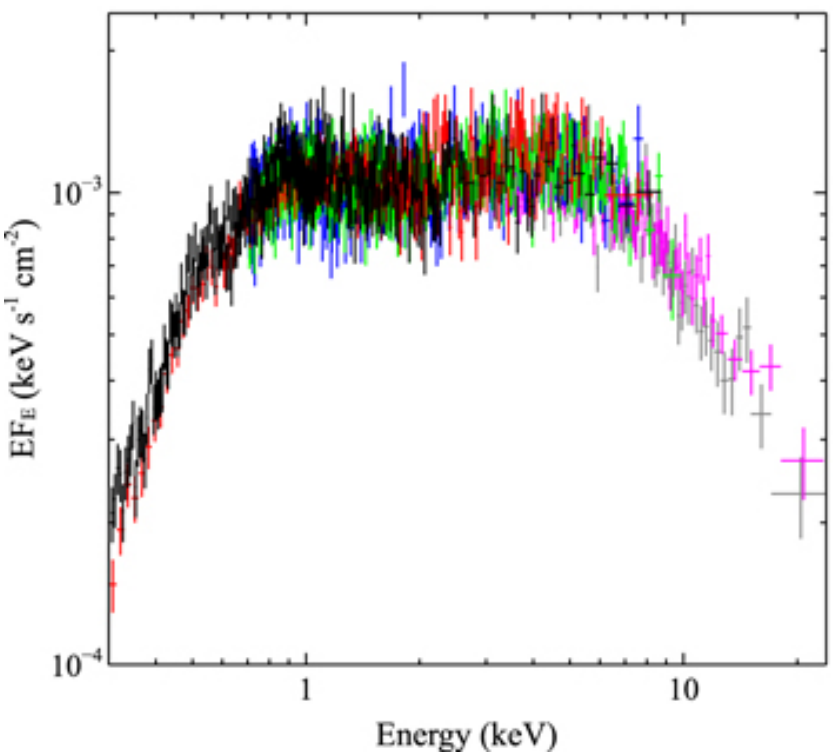

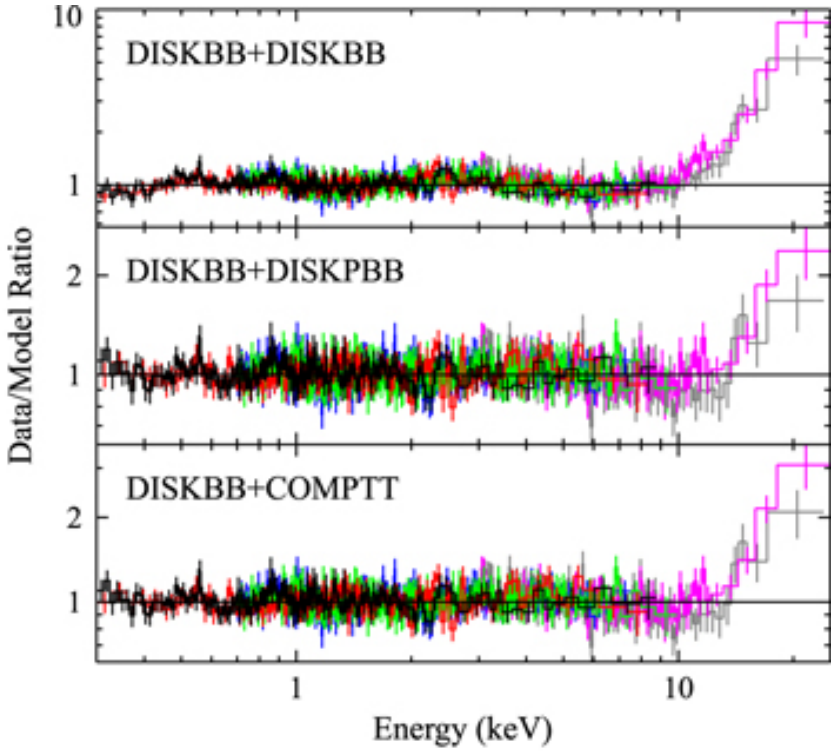

Geometry of an accretion flow from observations

Observed states in black hole binaries Esin + 1997

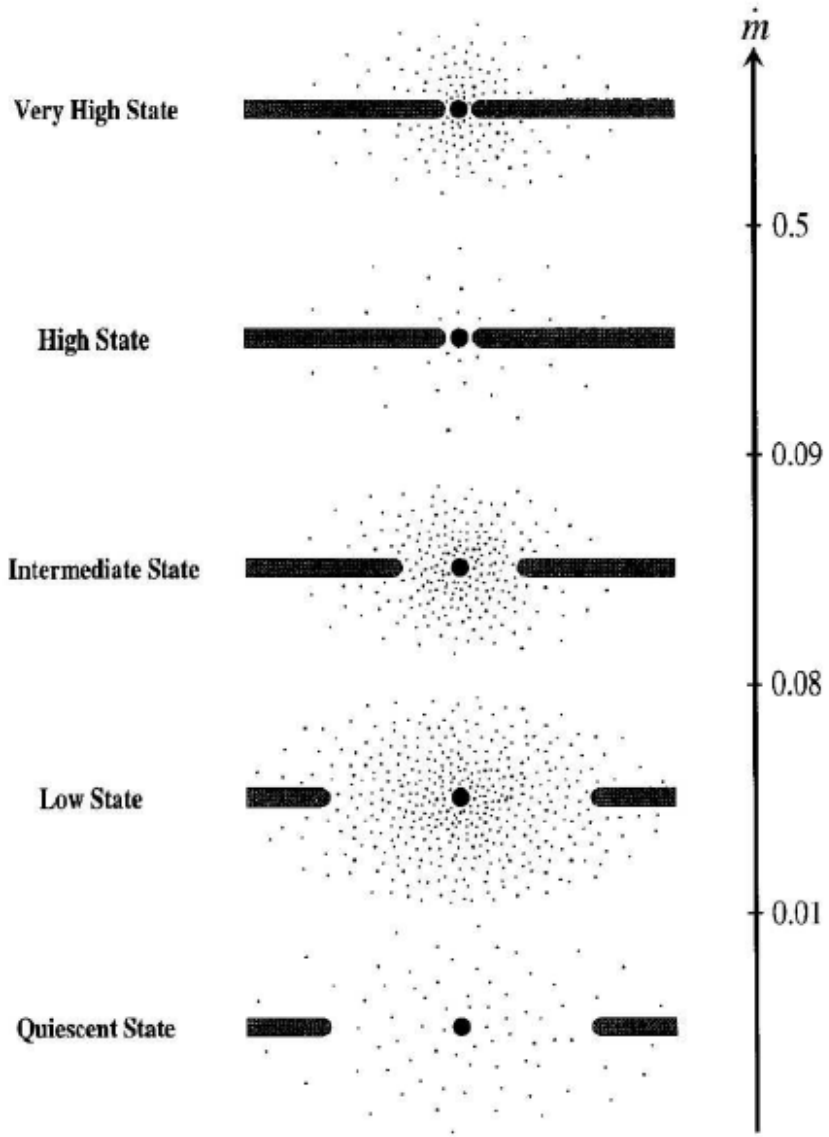

Geometry of an accretion flow from observations

Done + 2012

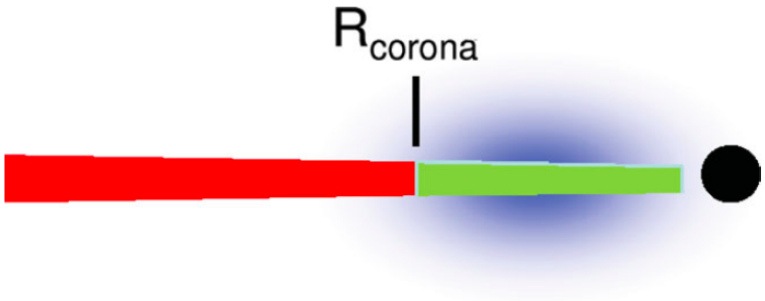

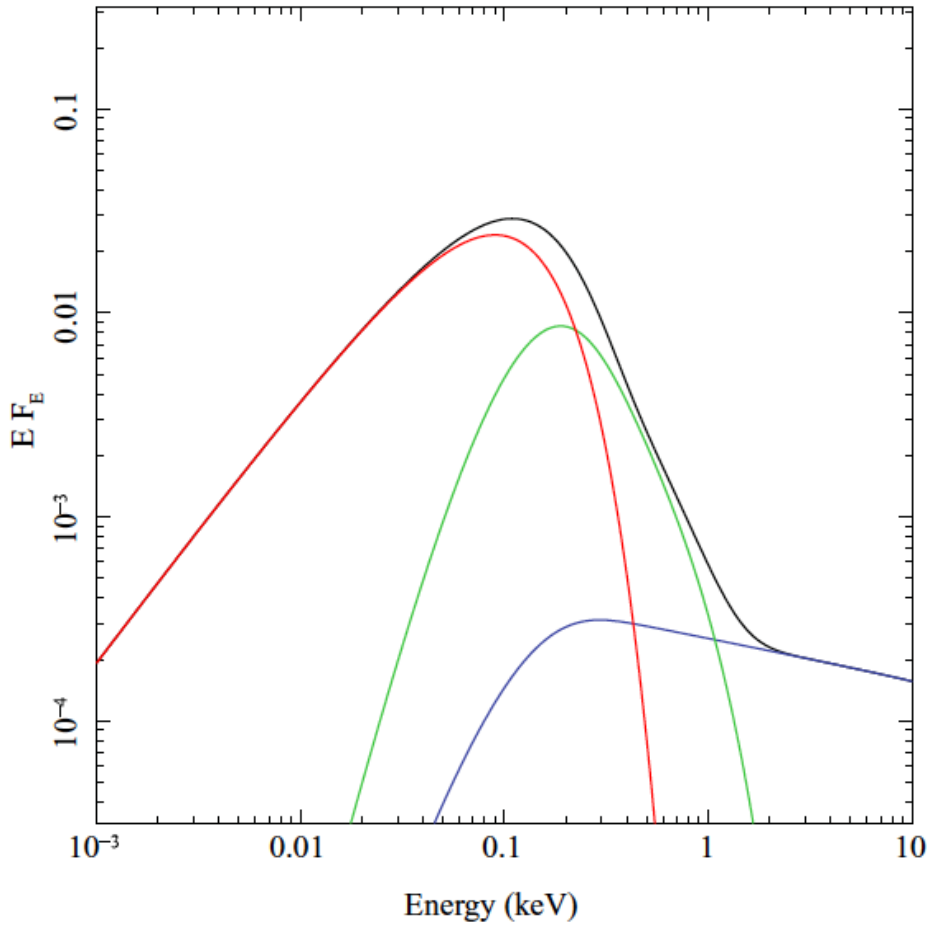

Geometry of an accretion flow from observations

Petrucci + 2013 for Mrk509

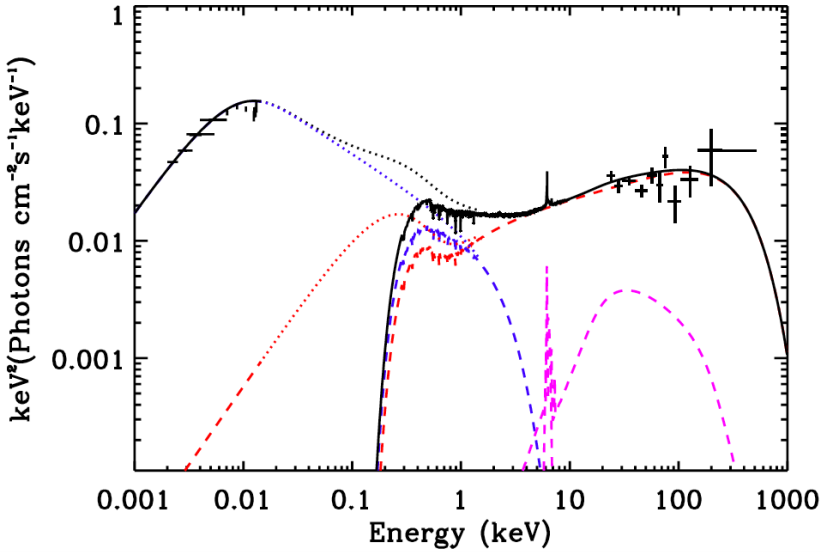

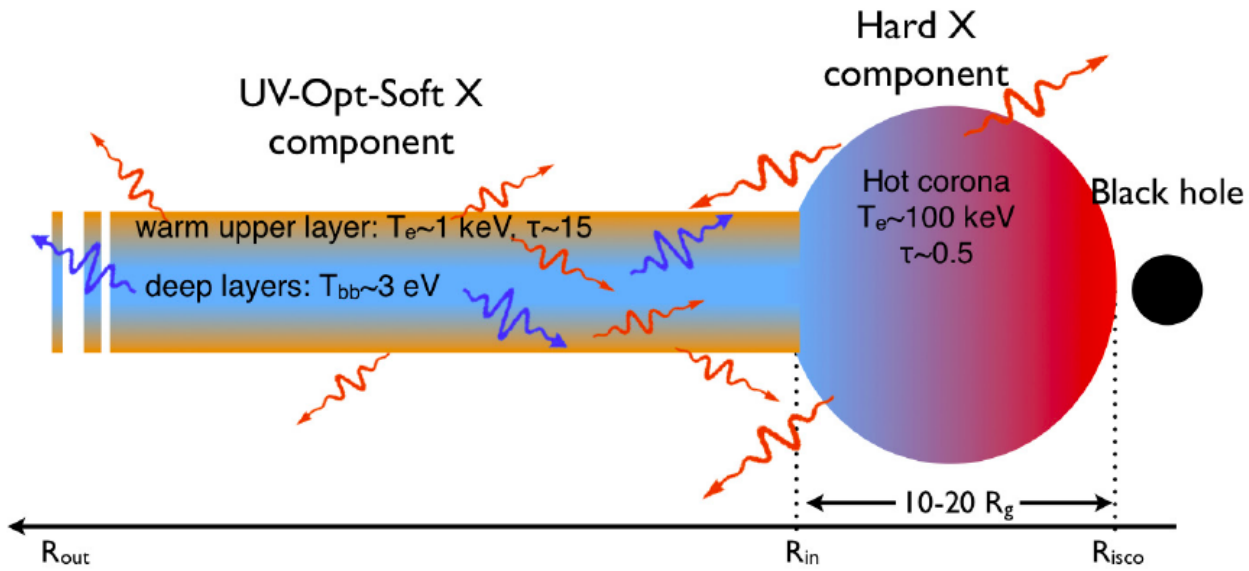

Radiative transfer equation, Różańska +08

$$\mu \frac{dI_\nu}{d\tau_\nu} = I_\nu - \frac{j_\nu}{\kappa_\nu + \sigma_\nu} = I_\nu - S_\nu$$

Emission coefficient j_ν is the sum of three terms, $j_\nu = j_\nu^{th} + j_\nu^{sc} + j_\nu^{fl}$.

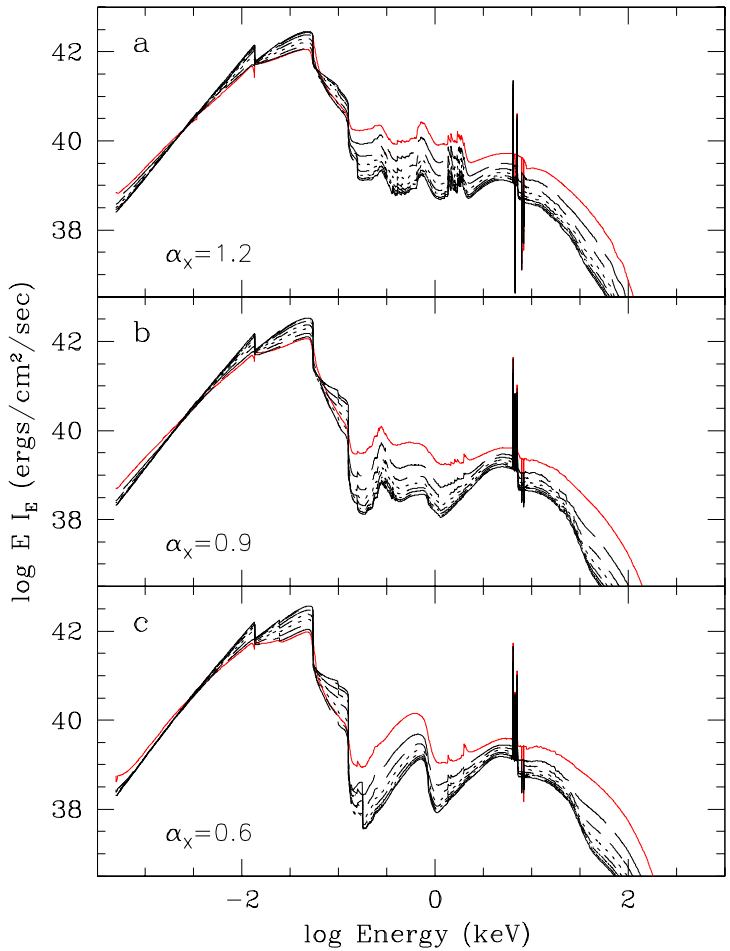

Radiative transfer equation, Różańska +08

$$\mu \frac{dI_\nu}{d\tau_\nu} = I_\nu - \frac{j_\nu}{\kappa_\nu + \sigma_\nu} = I_\nu - S_\nu$$

Emission coefficient j_ν is the sum of three terms, $j_\nu = j_\nu^{th} + j_\nu^{sc} + j_\nu^{fl}$.

Requires iteration with gas(X,Y,Z) structure due to equilibrium equations:

- Hydrostatic equil. $=> \frac{dP}{dz}$

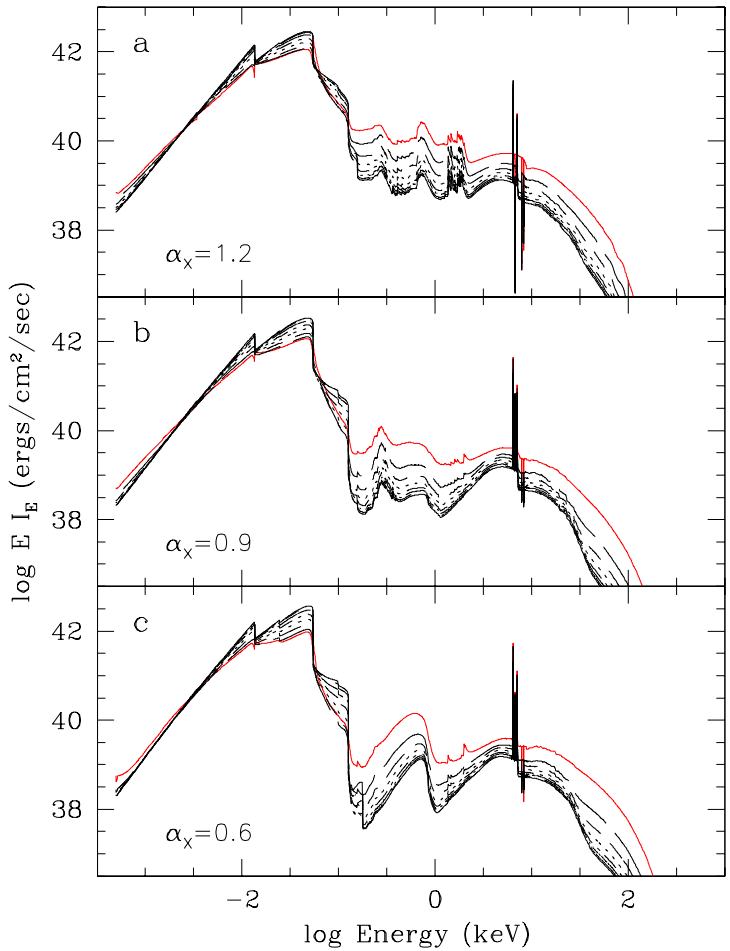

Radiative transfer equation, Różańska +08

$$\mu \frac{dI_\nu}{d\tau_\nu} = I_\nu - \frac{j_\nu}{\kappa_\nu + \sigma_\nu} = I_\nu - S_\nu$$

Emission coefficient j_ν is the sum of three terms, $j_\nu = j_\nu^{th} + j_\nu^{sc} + j_\nu^{fl}$.

Requires iteration with gas(X,Y,Z) structure due to equilibrium equations:

- Hydrostatic equil. $=> \frac{dP}{dz}$
- Radiative equil. $=> \frac{dT}{dz}$

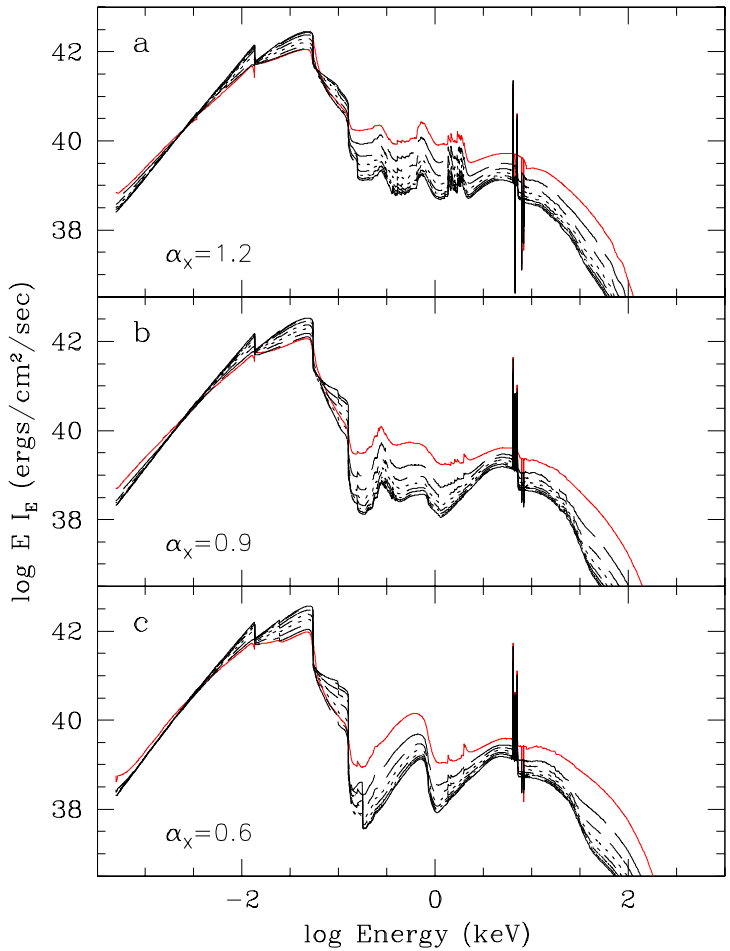

Radiative transfer equation, Różańska +08

$$\mu \frac{dI_\nu}{d\tau_\nu} = I_\nu - \frac{j_\nu}{\kappa_\nu + \sigma_\nu} = I_\nu - S_\nu$$

Emission coefficient j_ν is the sum of three terms, $j_\nu = j_\nu^{th} + j_\nu^{sc} + j_\nu^{fl}$.

Requires iteration with gas(X,Y,Z) structure due to equilibrium equations:

- Hydrostatic equil. $=> \frac{dP}{dz}$
- Radiative equil. $=> \frac{dT}{dz}$
- EoS - usually ideal gas

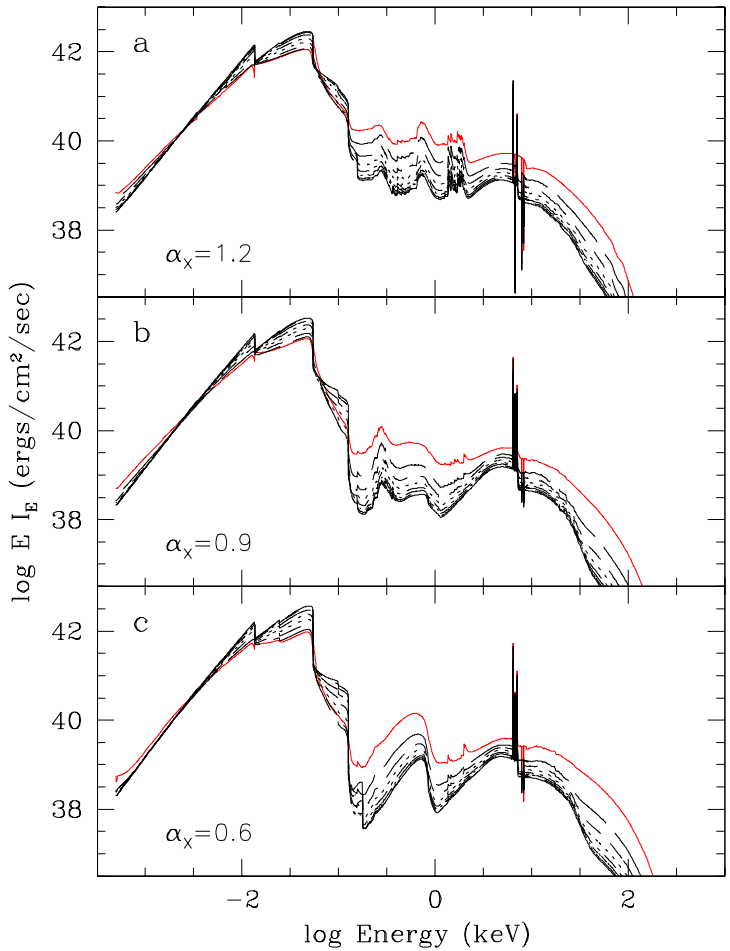

Model atmosphere calculations - glossary of terms

- Specific intensity I_ν, which flows through one cm^2 on the surface of an emitter into a direction. It is an intrinsic property of the source in erg cm^{-2} s^{-1} Hz^{-1} sr^{-1}.

Model atmosphere calculations - glossary of terms

1. Specific intensity I_ν, which flows through one cm^2 on the surface of an emitter into a direction. It is an intrinsic property of the source in $\mathrm{erg\ cm^{-2}\ s^{-1}\ Hz^{-1}\ sr^{-1}}$.
2. Energy dependent flux is the average of I_ν weighted by $\cos\theta$ (zenithal angle). Integration is over full solid angle 4π:

$$F_\nu = \oint I_\nu d\omega$$

It is an intrinsic property of the source in $\mathrm{erg\ cm^{-2}\ s^{-1}\ Hz^{-1}}$.

Model atmosphere calculations - glossary of terms

1. Specific intensity I_ν, which flows through one cm^2 on the surface of an emitter into a direction. It is an intrinsic property of the source in erg cm^{-2} s^{-1} Hz^{-1} sr^{-1}.
2. Energy dependent flux is the average of I_ν weighted by $\cos\theta$ (zenithal angle). Integration is over full solid angle 4π:

$$F_\nu = \oint I_\nu d\omega$$

   It is an intrinsic property of the source in erg cm^{-2} s^{-1} Hz^{-1}.
3. Infinitesimal energy $d\mathcal{F}_\nu$ can be measured by a distant observer in flat space, over infinitesimal part of full solid angle

$$d\mathcal{F}_\nu = I_\nu d\omega,$$

   subtended by the area as seen by an observer. It is NOT an intrinsic property of the source in erg cm^{-2} s^{-1} Hz^{-1}.

Spherically symmetric stars - ideal model of NS

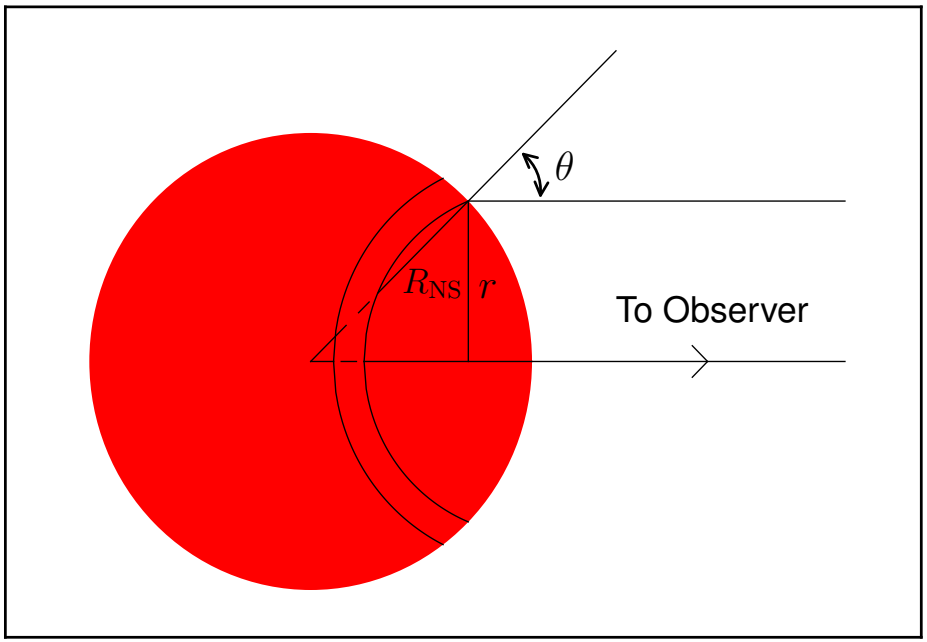

$$\mathcal{F}_{\nu,\rm NS} = \int_\Omega I_\nu d\omega = 2\pi \left(\frac{R_{\rm NS}}{D}\right)^2 \int_0^1 I_\nu \mu d\mu = \left(\frac{R_{\rm NS}}{D}\right)^2 F_\nu$$

The observed intensity per detector area is proportional to the flux emitted locally from 1 cm^2 of the star's surface, only due to the spherical shape of the emitting region. Mihalas 1976.

Axially symmetric accretion disk - Shakura & Sunyaev 1973

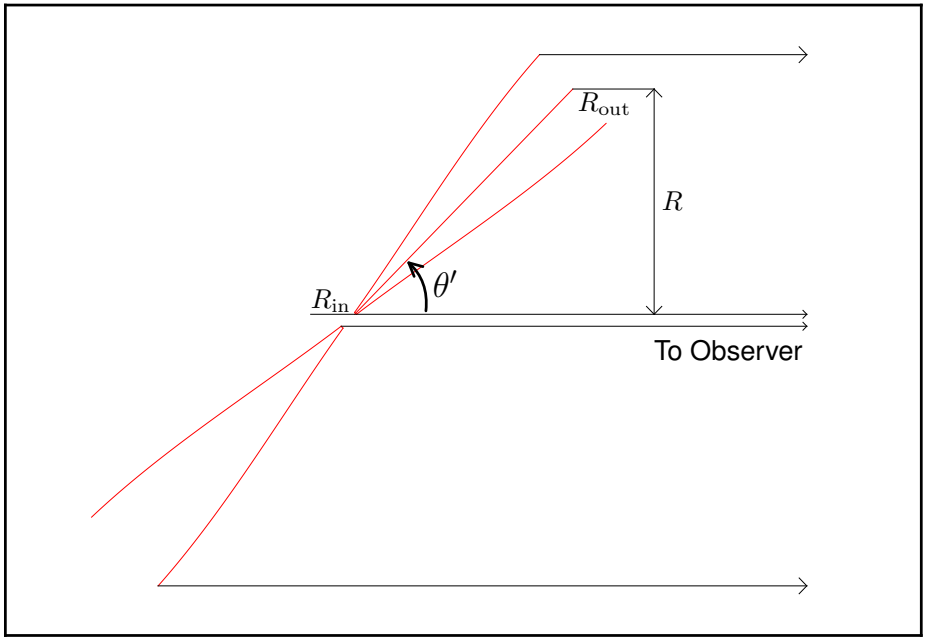

$$\mathcal{F}_{\nu,\rm AD} = \int_\Omega I_\nu d\omega = 2\pi \frac{\sin\theta'}{D^2} \int_{R_{\rm in}}^{R_{\rm out}} I_\nu R dR,$$

Monochromatic intensity, I_ν emitted in the specific direction is integrated over the disk surface from the inner to outer disk radii.

Neutron star with an accretion disk, Różańska +17

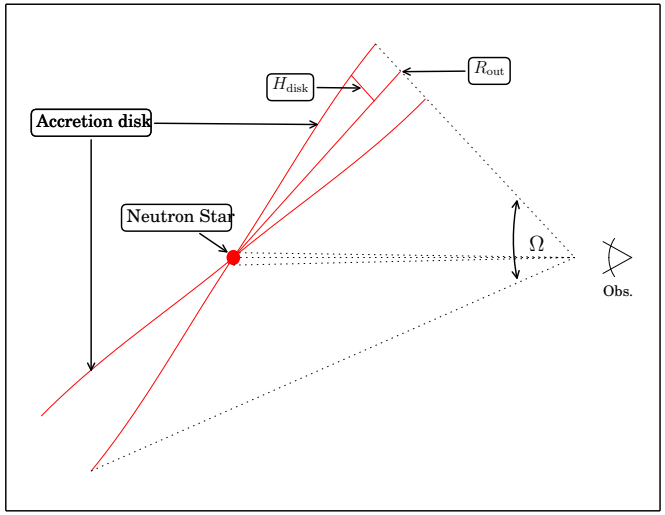

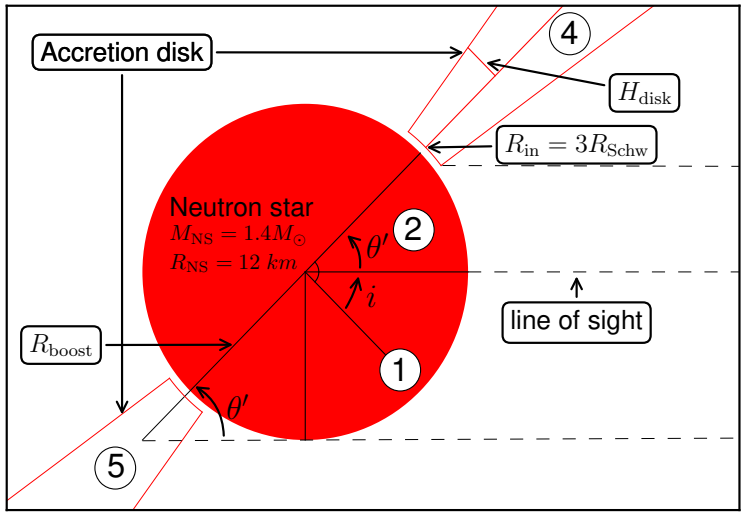

$$\mathcal{F}_{\nu,\mathrm{All}} = \left(\frac{1}{D}\right)^2 \left[\pi R_{\mathrm{NS}}^2 \left(\int_0^1 I_\nu \mu d\mu + \int_{\cos\theta'}^1 I_\nu \mu d\mu\right)\right.$$
$$+ 2\left(\int_0^{R_{\mathrm{NS}}} I_\nu \sin\theta' \sqrt{R_{\mathrm{NS}}^2 - x^2}\, dx - \int_0^{R_{\mathrm{NS}}\sin\theta'} I_\nu \sqrt{R_{\mathrm{NS}}^2 \sin^2\theta' - x^2}\, dx\right)$$
$$\left. + \pi \sin\theta' \left(\int_{R_{\mathrm{in}}}^{R_{\mathrm{out}}} I_\nu R dR + \int_{R_{\mathrm{boost}}}^{R_{\mathrm{out}}} I_\nu R dR\right)\right]$$

LMXB at different viewing angles, Różańska +17

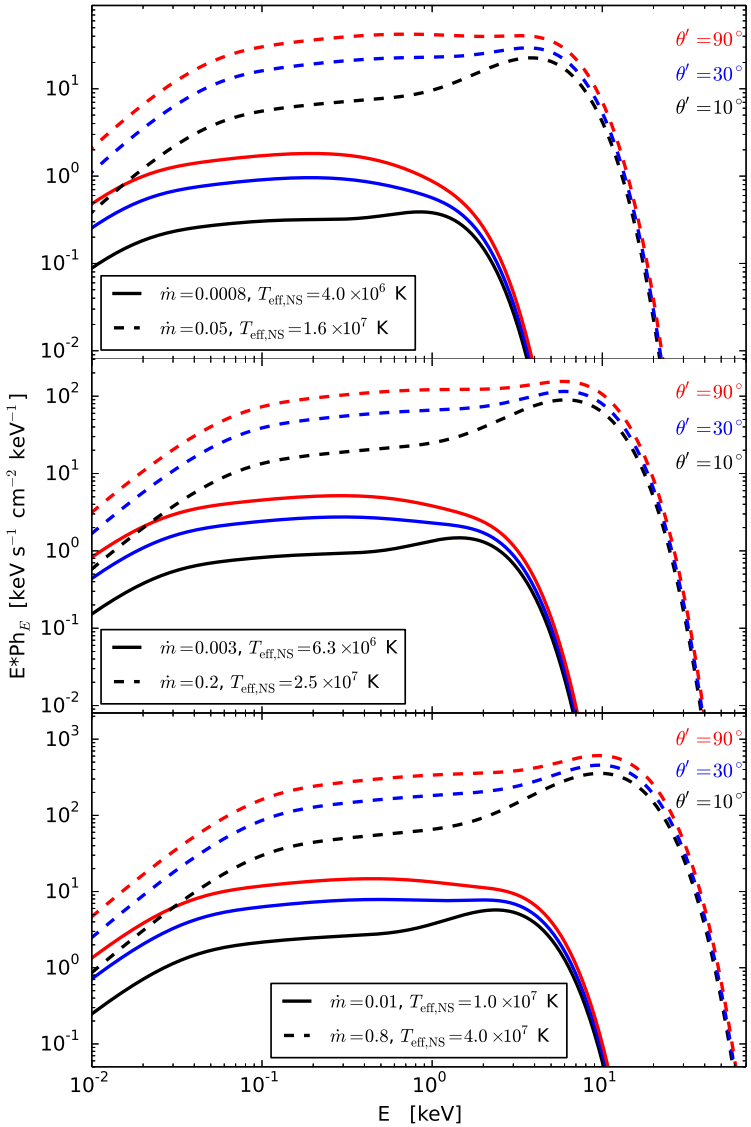

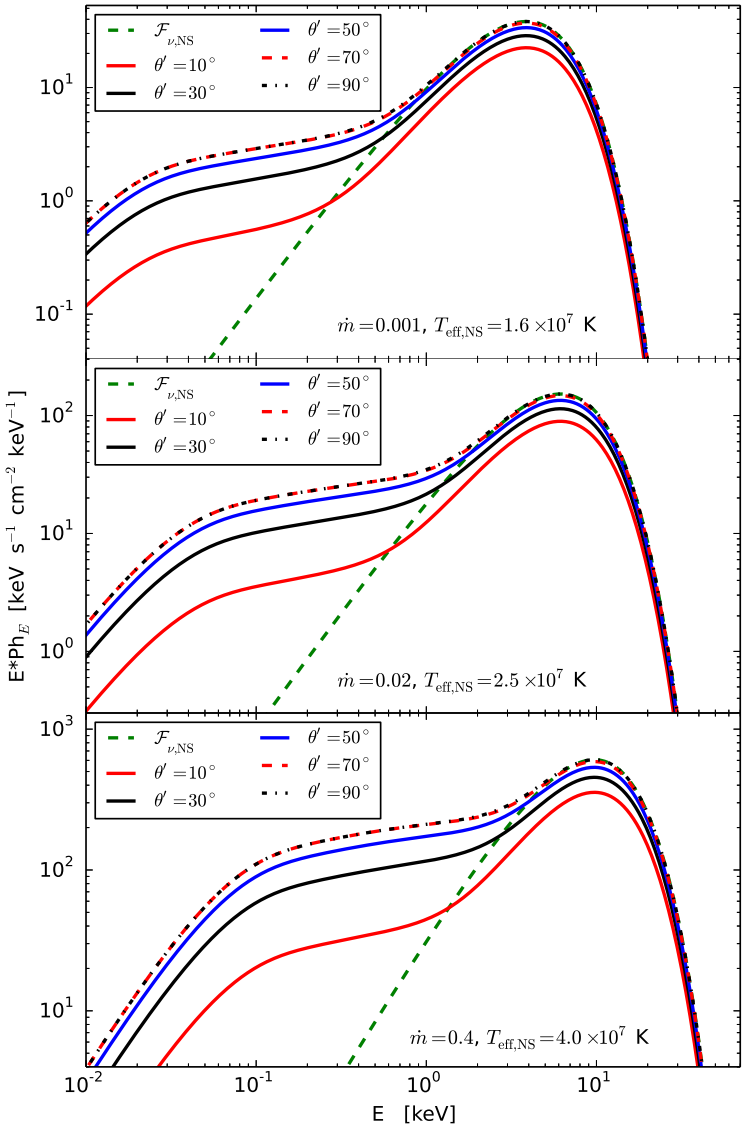

The influence of the viewing angle

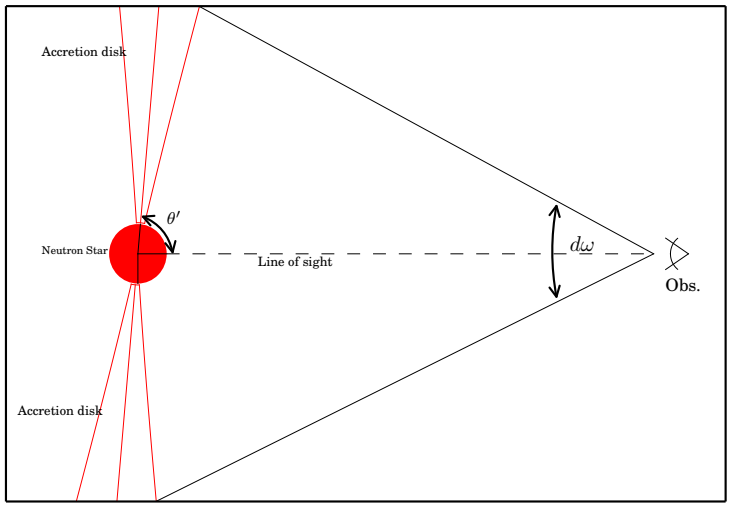

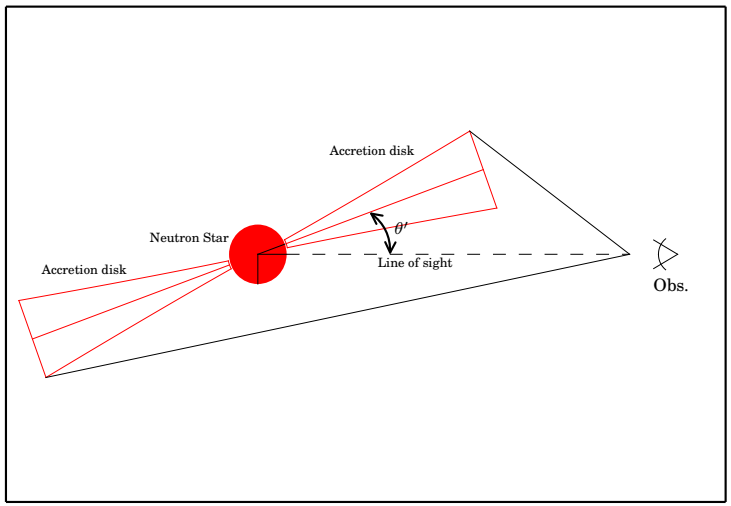

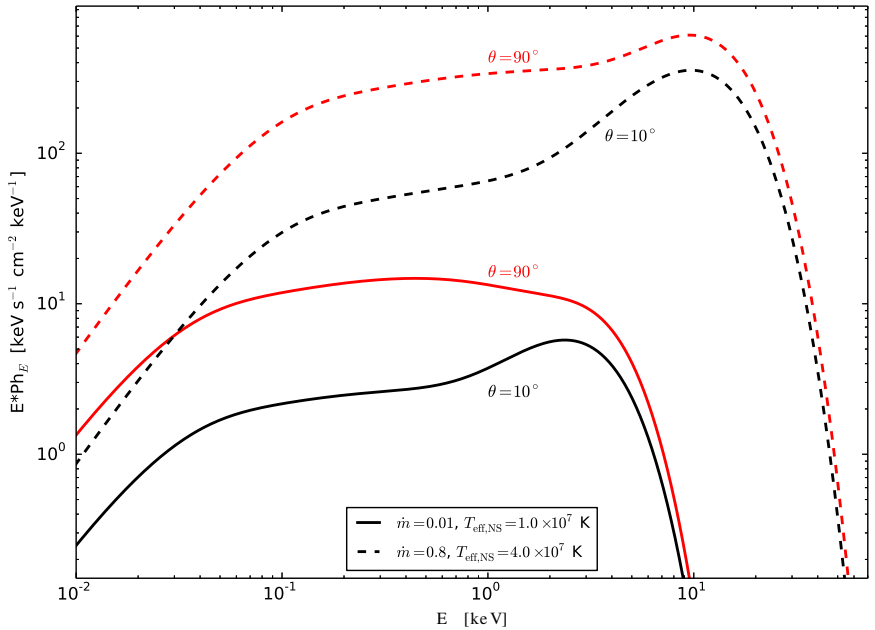

Black line - edge on

Red line - face on

The size of inner region, Różańska +18

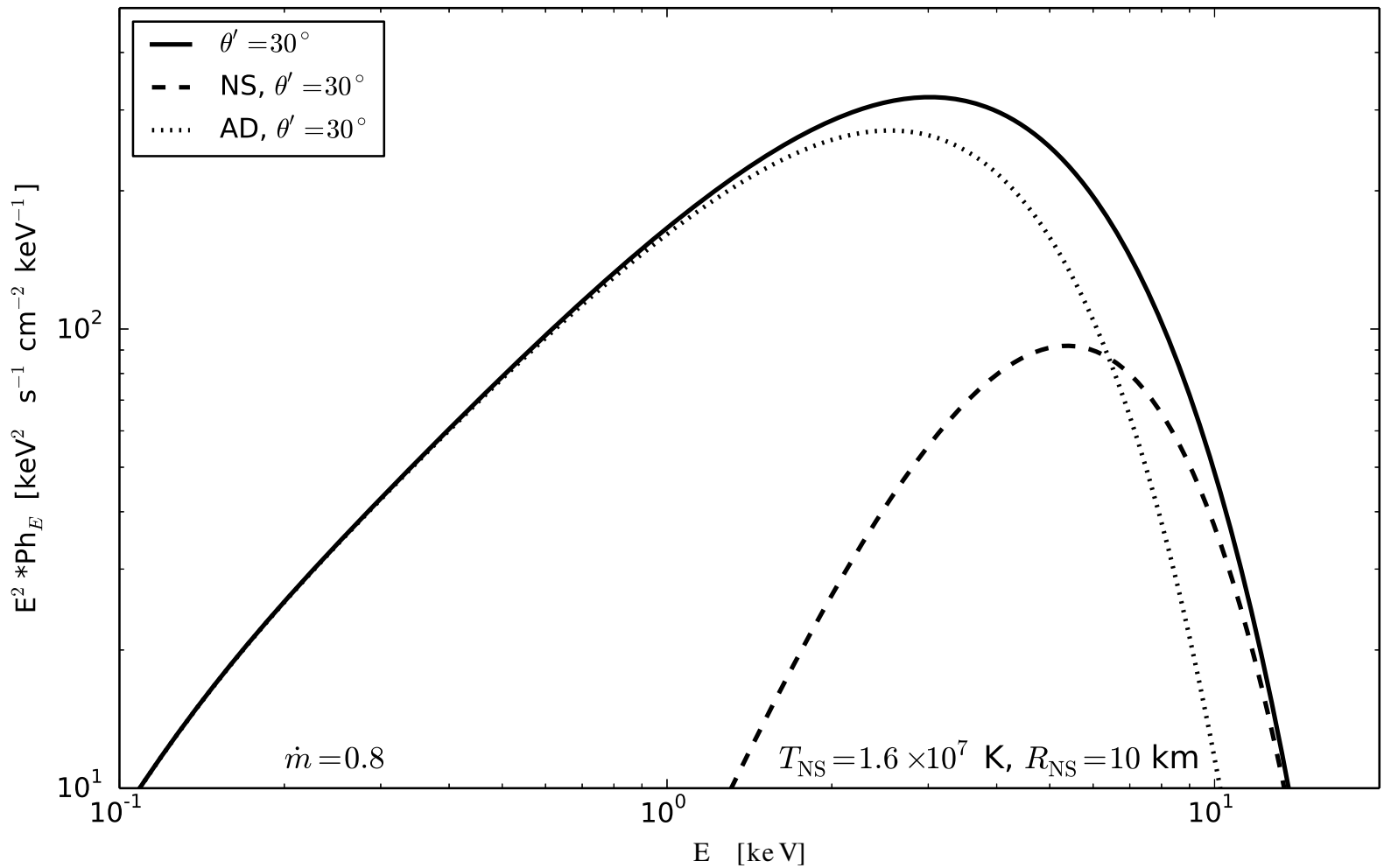

The size of inner region, Różańska +18

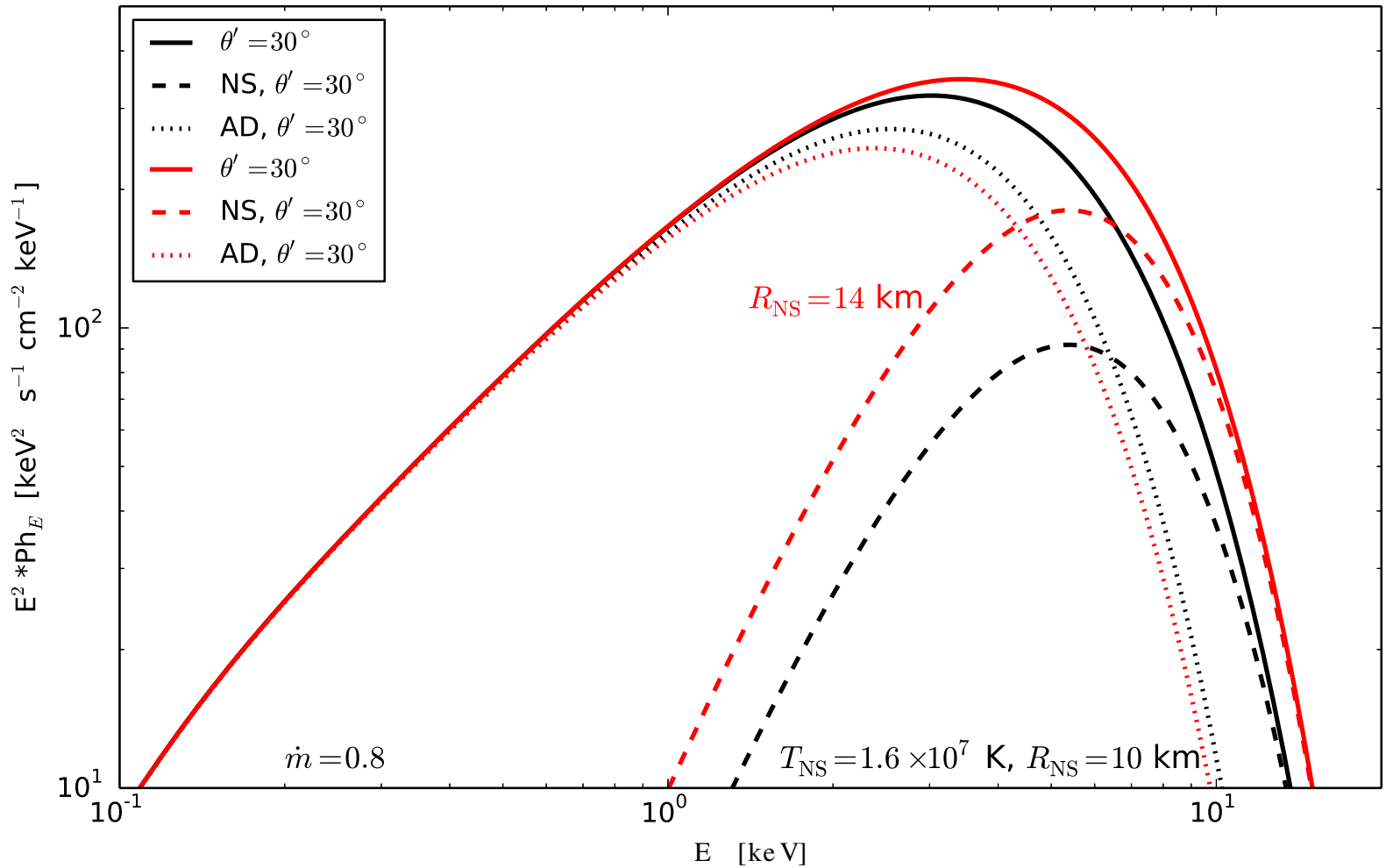

X-ray observations of XTE J1709-267 by *XMM-Newton*

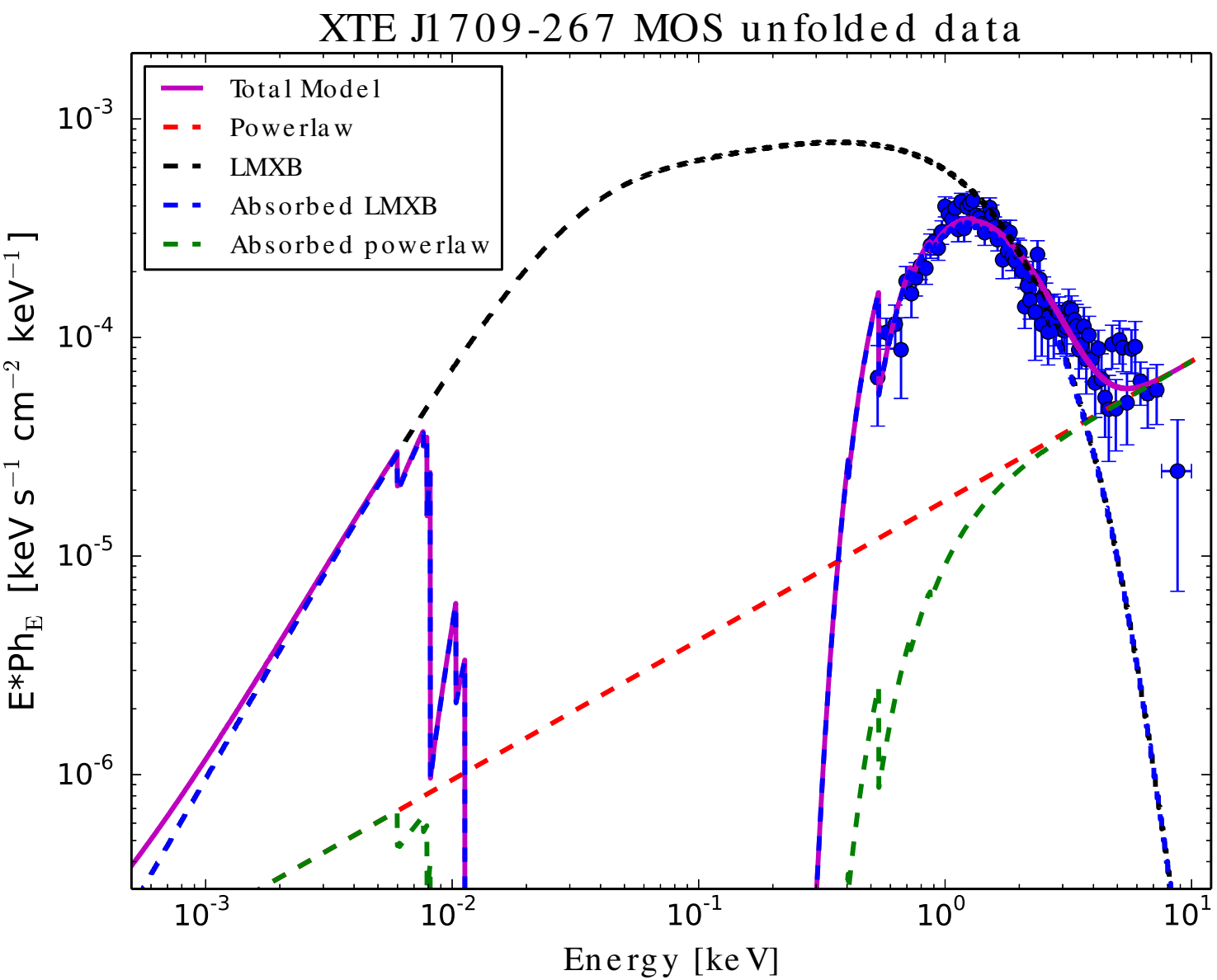

NUSTAR/XMM-Newton data of ULXs, Różańska +18

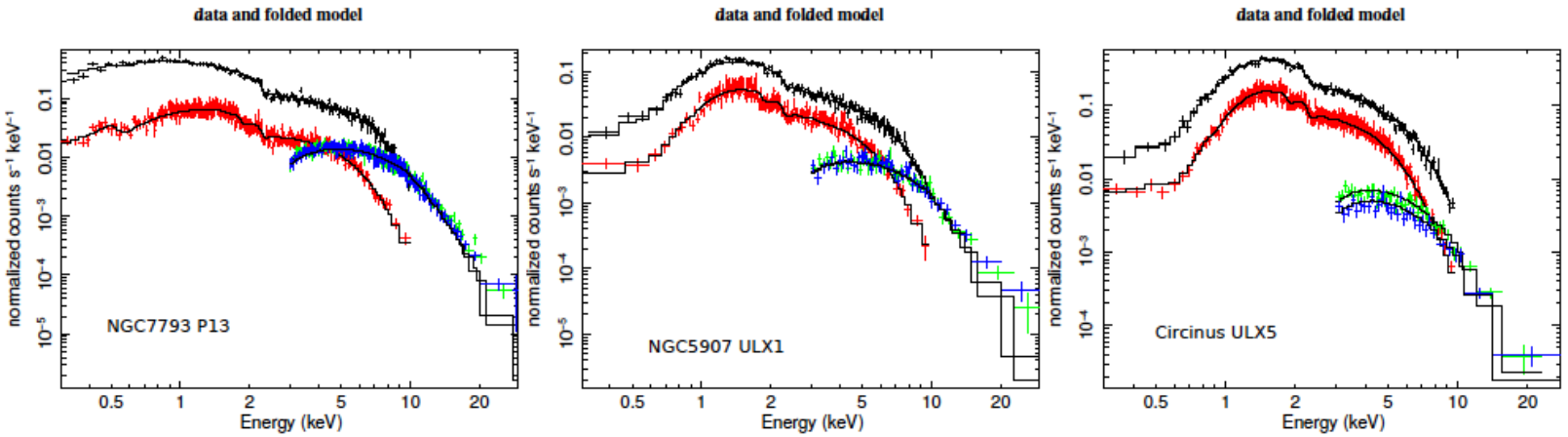

Fig. 1. Normalized counts from all detectors used in our spectral fitting analysis for P13, ULX1, and ULX5 respectively. Black and red crosses correspond to the *XMM-Newton* detectors EPIC-pn and EPIC-MOS. Green and blue crosses are data from *NuSTAR* FPMA and FPMB respectively. Black solid lines are the best fitted models.

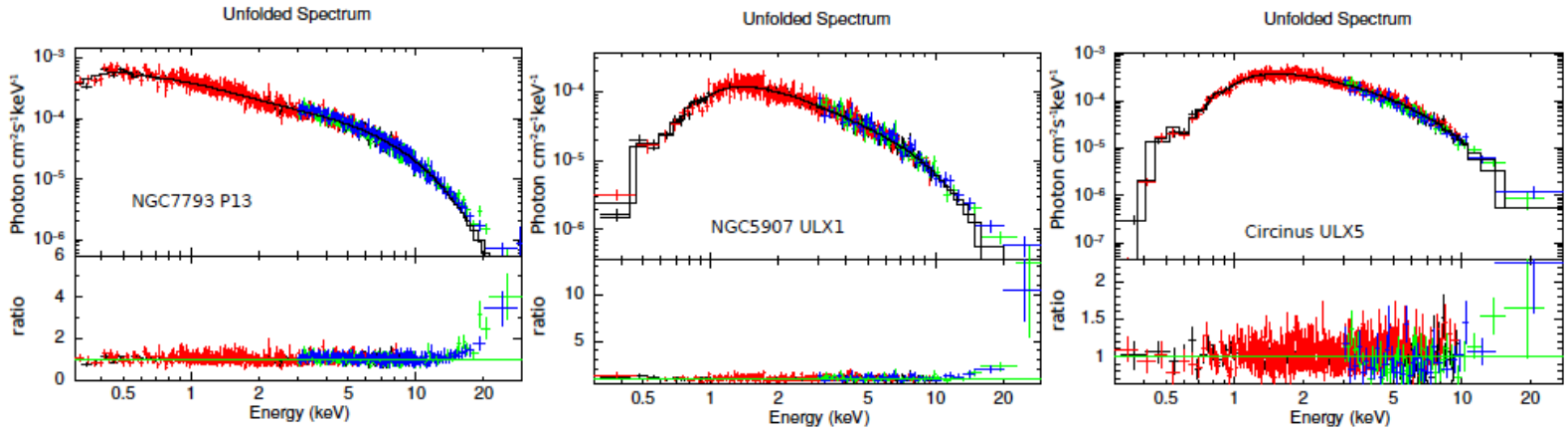

Fig. 2. Upper panels shows unfolded photon spectra from all detectors used in our spectral fitting analysis, while lower panels present the ratio i.e. data divided by model. All colors have the same meaning as in Fig. 1.

NUSTAR/XMM-Newton data of ULXs, Różańska +18

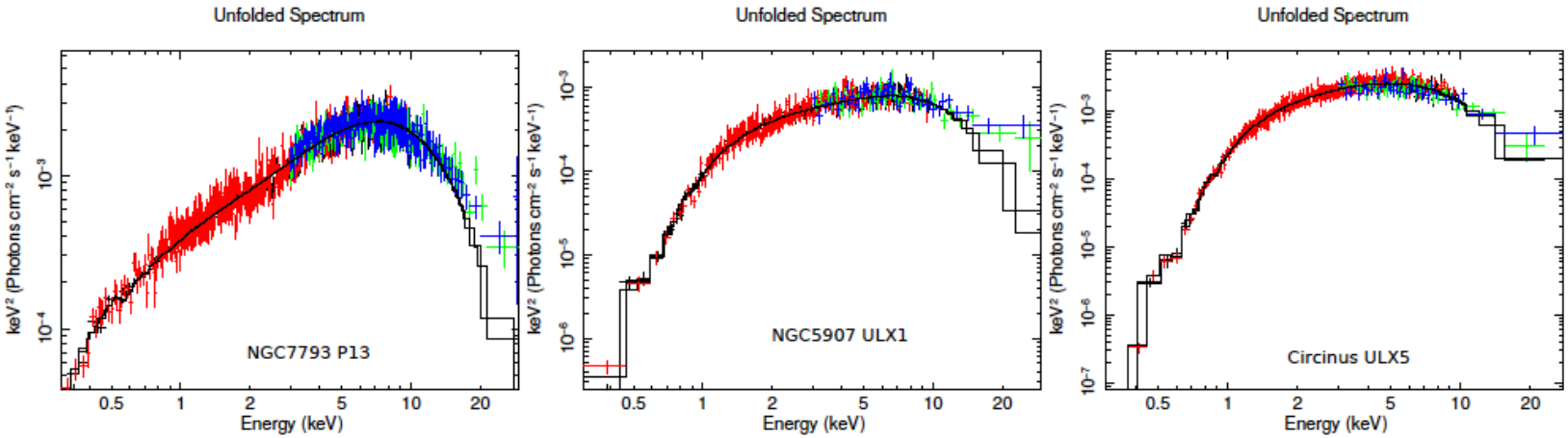

Fig. 3. Unfolded energy spectrum from all detectors used in our spectral fitting analysis. $E * F_{\rm E}$ quantity is plotted to show the maximum emission from hard energy tail which is associated with the emission. Black and red crosses correspond to the *XMM-Newton* detectors EPIC-pn and EPIC-MOS. Green and blue crosses are data from *NuSTAR* FPMA and FPMB respectively. Black solid lines are the best fitted models.

The single model consists of two emitting regions with mutual attenuation taken into account. The statistic is extremely good:

Src. Name	NGC7793 P13	NGC5907 ULX1	Circinus ULX5
χ^2	1.08	1.01	1.14

Fitting parameters with the *tbnew*nsmcbb* model.

Src.	Model	Parameter	Value	Unit
P13	*tbnew*	$N_{\rm H}$	$4.77^{+0.45}_{-0.44} \times 10^{20}$	$\rm cm^{-2}$
	nsmcbb	$T_{\rm eff,NS}$	$1.819 \pm 0.025 \times 10^{7}$	K
	nsmcbb	$T_{\rm in}$	$1.215^{+0.036}_{-0.046} \times 10^{7}$	K
	nsmcbb	θ'	10 ± 6.59	deg
	nsmcbb	N	$8.62 \pm 0.54 \times 10^{-6}$	–
ULX1	*tbnew*	$N_{\rm H}$	$4.45^{+0.13}_{-0.2} \times 10^{21}$	$\rm cm^{-2}$
	nsmcbb	$T_{\rm eff,NS}$	$1.776^{+0.071}_{-0.032} \times 10^{7}$	K
	nsmcbb	$T_{\rm in}$	$9.014^{+2.809}_{-0.244} \times 10^{6}$	K
	nsmcbb	θ'	70 ± 1.87	deg
	nsmcbb	N	$2.33^{+0.70}_{-0.42} \times 10^{-6}$	–
ULX5	*tbnew*	$N_{\rm H}$	$5.97^{+0.01}_{-0.01} \times 10^{21}$	$\rm cm^{-2}$
	nsmcbb	$T_{\rm eff,NS}$	$1.633^{+0.117}_{-0.109} \times 10^{7}$	K
	nsmcbb	$T_{\rm in}$	$1.261^{+0.398}_{-0.075} \times 10^{7}$	K
	nsmcbb	θ'	$12.49^{+1.74}_{-0.71}$	deg
	nsmcbb	N	$15.23 \pm 0.94 \times 10^{-6}$	–

Distance from the model normalization, Różańska +18

Src.	Parameter	Value	Unit
P13	χ^2/dof	1344/1245	–
	$F_{\rm X}$(2-10 keV)	4.36 $\times 10^{-12}$	erg s^{-1} cm^{-2}
	$F_{\rm X}$(0.3-30 keV)	6.83 $\times 10^{-12}$	erg s^{-1} cm^{-2}
	$D = 10/\sqrt{N}$	$\mathbf{3.41}^{+0.11}_{-0.10}$	Mpc
	$L_{\rm X}$(0.3-30 keV)	9.59 $\times 10^{39}$	erg s^{-1}
ULX1	χ^2/dof	867/859	–
	$F_{\rm X}$(2-10 keV)	1.73 $\times$ 10^{-12}	erg s^{-1} cm^{-2}
	$F_{\rm X}$(0.3-30 keV)	2.81 $\times$ 10^{-12}	erg s^{-1} cm^{-2}
	$D = 10/\sqrt{N}$	$\mathbf{6.55}^{+0.69}_{-0.81}$	Mpc
	$L_{\rm X}$(0.3-30 keV)	1.49 $\times$ 10^{40}	erg s^{-1}
ULX5	χ^2/dof	872/762	–
	$F_{\rm X}$(2-10 keV)	5.78 $\times$ 10^{-12}	erg s^{-1} cm^{-2}
	$F_{\rm X}$(0.3-30 keV)	9.18 $\times$ 10^{-12}	erg s^{-1} cm^{-2}
	$D = 10/\sqrt{N}$	$\mathbf{2.60}^{+0.05}_{-0.03}$	Mpc
	$L_{\rm X}$(0.3-30 keV)	7.49 $\times$ 10^{39}	erg s^{-1}

Distance from the model normalization, Różańska +18

In case of two ULXs the distant determination from our method agrees with previous measurements:

Src. Name	NGC7793 P13	NGC5907 ULX1	Circinus ULX5
D [Mpc]	$\mathbf{3.41}^{+0.11}_{-0.10}$	$6.55^{+0.69}_{-0.81}$	$\mathbf{2.60}^{+0.05}_{-0.03}$
Previous distances	3.9 C. **3.4** C.	13 T. 17 T.	4 T. **2.79** RV.
Method	Cepheid	Tully	Radial Vel.
Ref.	Pietrzyński +10	Tully +16	Koribalski +04

Conclusions

- ULXs may contain hot neutron star in the center

Conclusions

1. ULXs may contain hot neutron star in the center
2. The successful fit with single model component allows for distant determination

Conclusions

1. ULXs may contain hot neutron star in the center
2. The successful fit with single model component allows for distant determination
3. We aimed to show purely geometrical effect

Conclusions

1. ULXs may contain hot neutron star in the center
2. The successful fit with single model component allows for distant determination
3. We aimed to show purely geometrical effect
4. Any double bump observed in X-rays may be an evidence of two emitting regions and non-spherical source geometry

Conclusions

1. ULXs may contain hot neutron star in the center
2. The successful fit with single model component allows for distant determination
3. We aimed to show purely geometrical effect
4. Any double bump observed in X-rays may be an evidence of two emitting regions and non-spherical source geometry
5. **ATHENA will provide continuum curvature for those source, in soft X-ray energy end**

ATHENA simulated spectrum for WFI detector

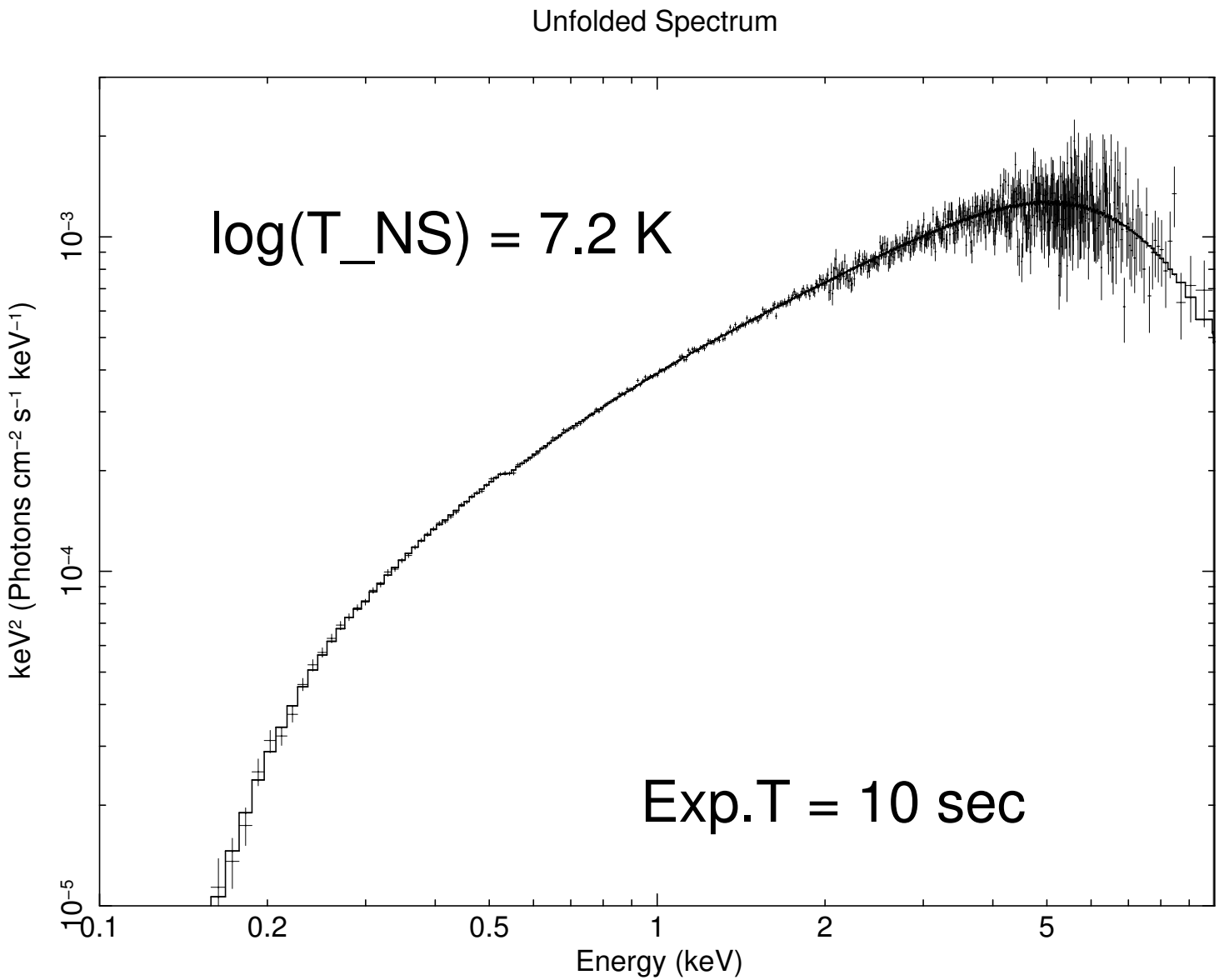

ATHENA simulated spectrum for WFI detector

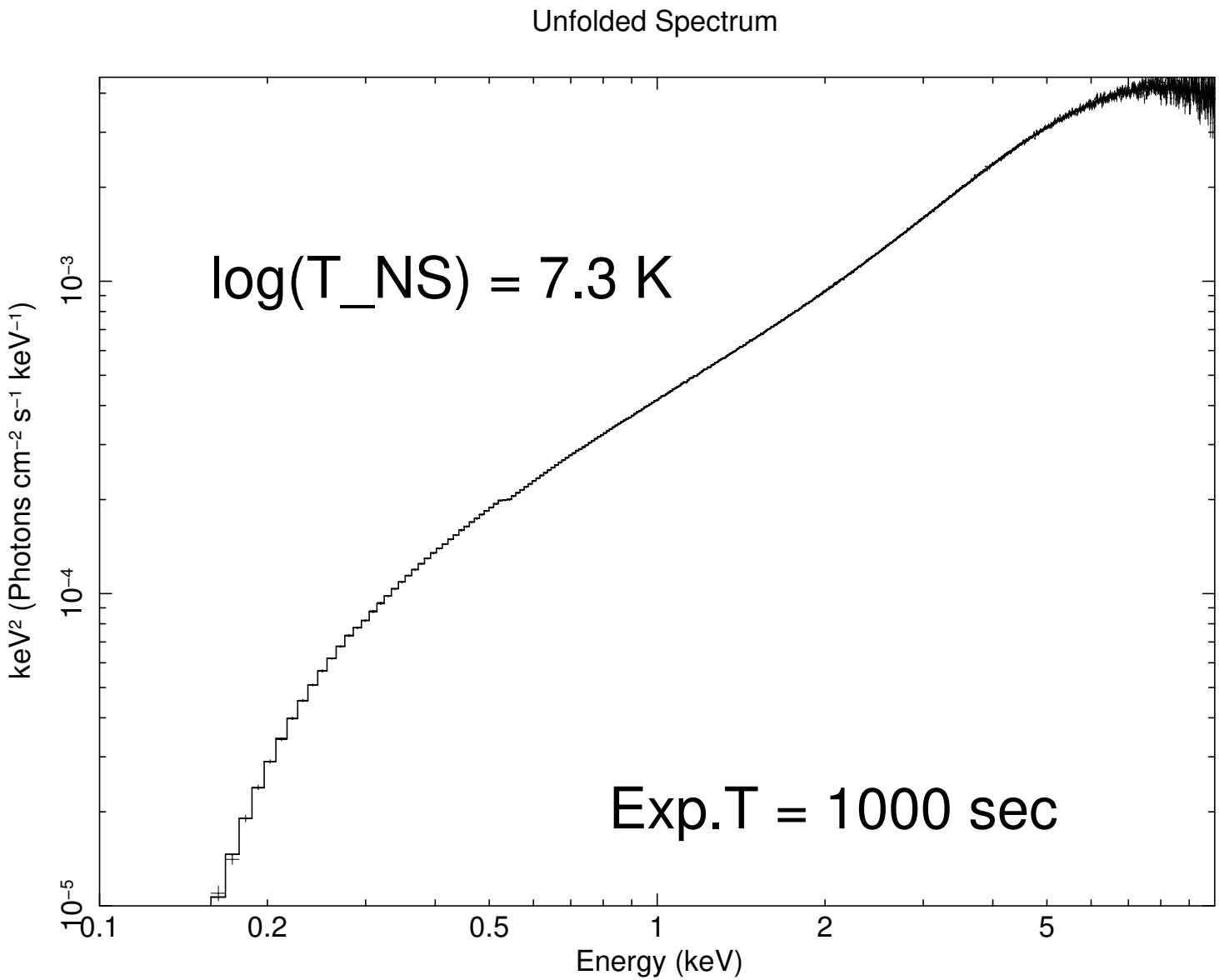

AGN, Petrucci et al. 2013

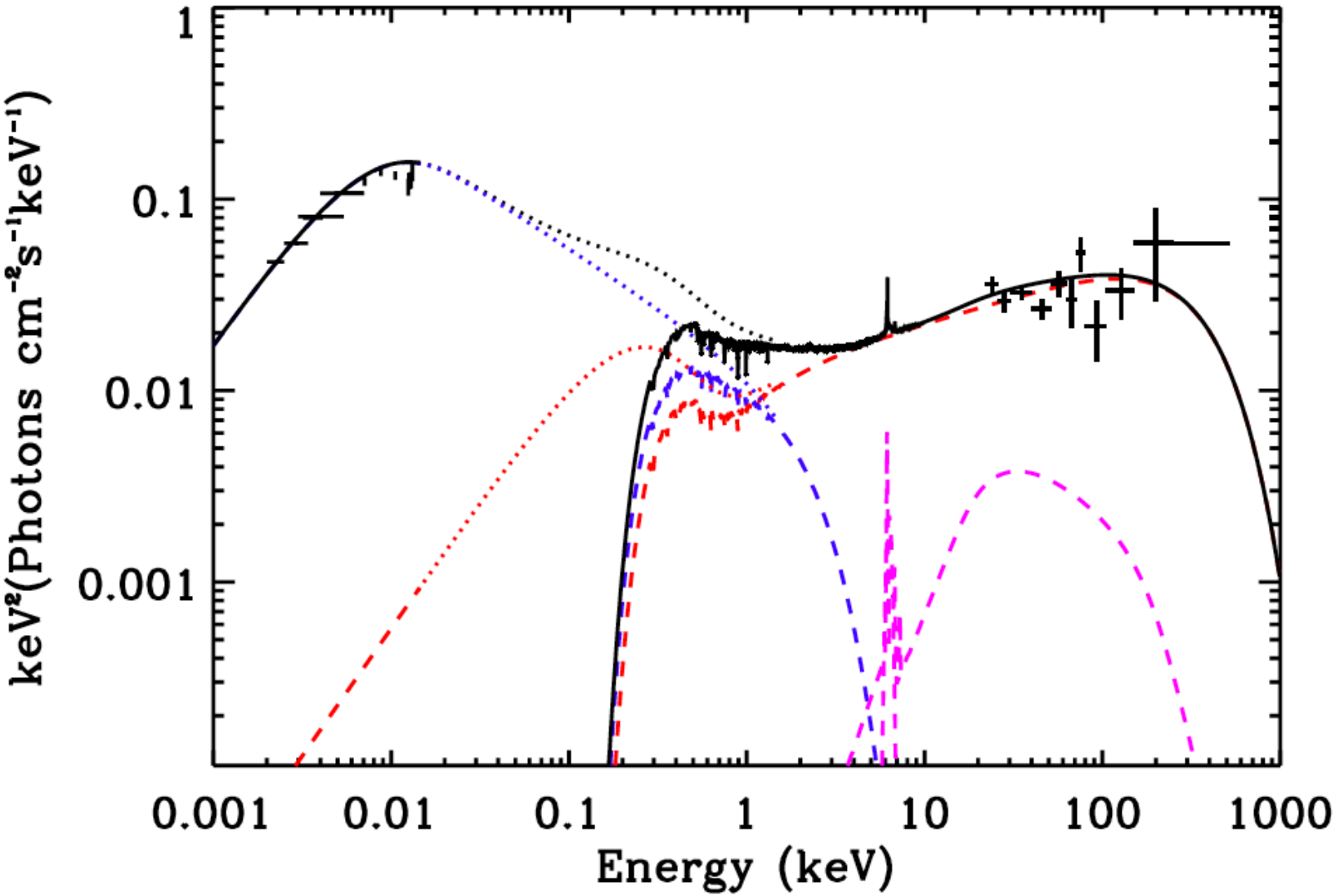

Activities on ATHENA mission in Poland

1. Poland works on four subsystems for **ATHENA**:
   - **Filter Wheel** for **WFI**
   - **Power Distribution Unit** for **WFI**
   - **Dewar Door** for **X-IFU**
   - **Power Distribution Unit** for **X-IFU**
2. I have written Activity Proposals for those actions, and finally **Project Experiment Agreement** - recently signed with **ESA**
3. I have formed **Polish Scientific Consortium** - the first meeting is on Oct. 24^{th}
4. Recently the contract for **Visibility Study** of **SIM** was signed with **ESA** - the project dedicated for Polish Industry - on good way to design and build **SIM** in the future

The inner optically thick source of $T \sim 1$ keV is compact

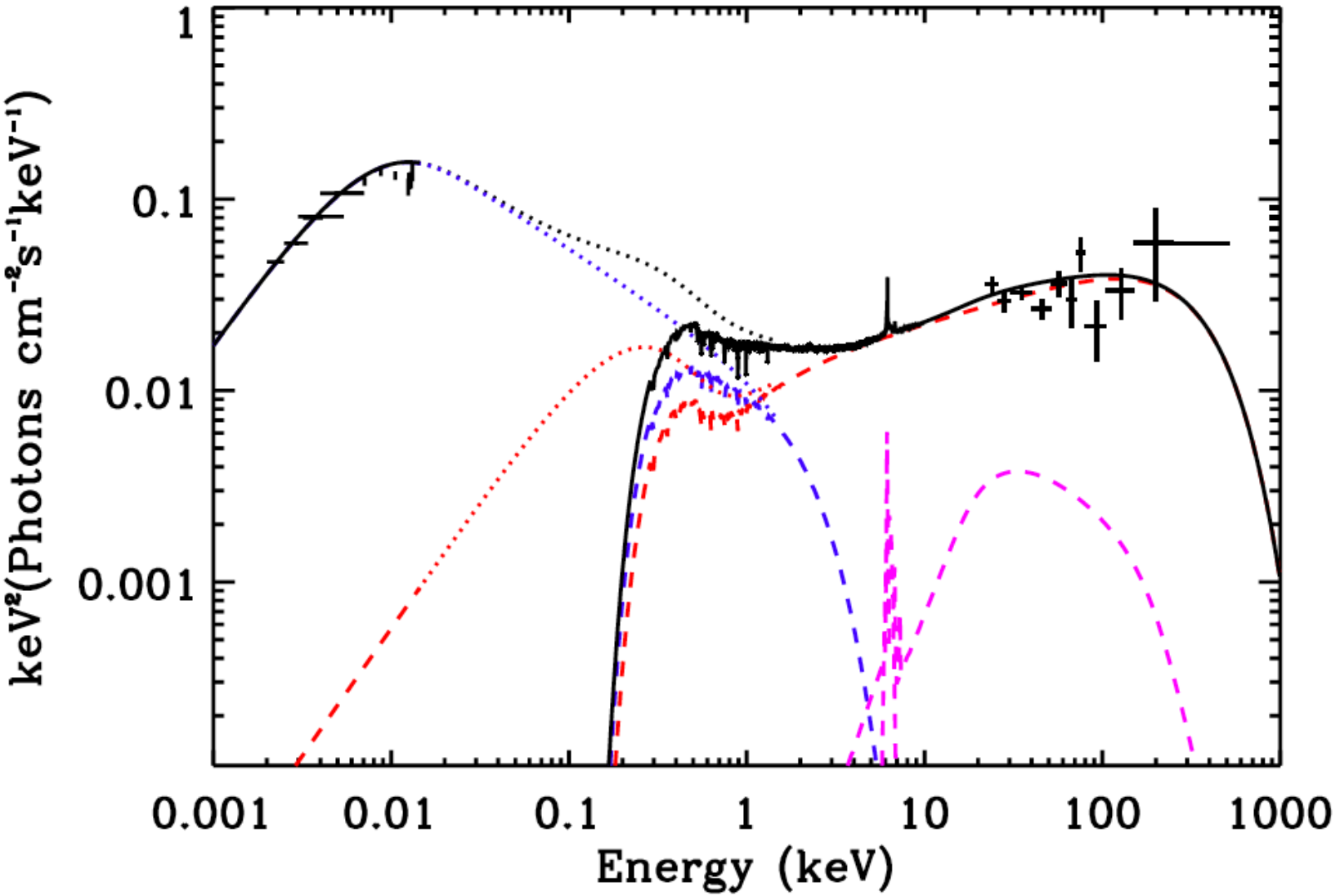

The inner optically thick source of $T \sim 1$ keV is compact